International Conference on Space Optics—ICSO 2022

Dubrovnik, Croatia

3–7 October 2022

Edited by Kyriaki Minoglou, Nikos Karafolas, and Bruno Cugny,

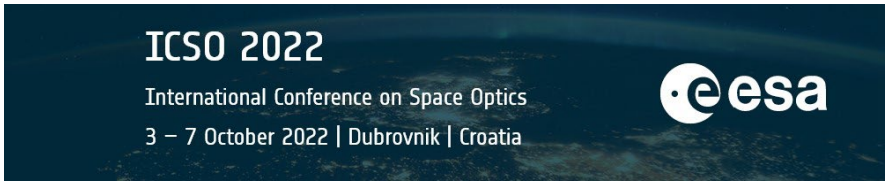

Towards a spatial light modulator technology for space applications: performance analysis under the environmental conditions

International Conference on Space Optics — ICSO 2022, edited by Kyriaki Minoglou, Nikos Karafolas, Bruno Cugny, Proc. of SPIE Vol. 12777, 127773U · © 2023 ESA and CNES · 0277-786X · doi: 10.1117/12.2690567

Towards a spatial light modulator technology for space applications: performance analysis under the environmental conditions

S. Francés González*[a], D. Berndt[a], G. Borque Gallego[b], D. Borrelli[c], U. Dauderstädt[a], P. Dürr[a], M. Eckert[a], J. Heber[a], D. Kunze[a], C. Pache[b], Giuseppe Pilato[c], V. Raimondi[d], E. Suetta[c], H. Torlee[a], A. Ummel[b], M. Wagner[a]

[a] IPMS – Fraunhofer-Institut, Dresden, Germany; [b] CSEM, Centre Suisse d'Electronique et Microtechnique, Neuchâtel, Switzerland; [c] LEONARDO S.p.A., Campi Bisenzio (FI), Italy; [d] CNR – IFAC, Istituto di Fisica Applicata "Nello Carrara", Sesto Fiorentino (FI), Italy

ABSTRACT

Spatial Light Modulator (SLM) technologies are well established in many application fields over the last decades. Addressing challenging operational conditions, a special class of high-speed SLMs has emerged over the past 20 years, namely Micromirror Array (MMA) devices. Fraunhofer IPMS MMA technology has enabled several ultraviolet photolithography applications at industrial scale. Given the fact that these devices are available for scientific testing, we proposed to explore for the first time their functionality and performance with respect to the space application requirements for the European framework cooperation. Previous studies strongly support this approach with the investigation of several SLM technologies for space instrumentation.

In this study, the key parameters of an already available 256 x 256 pixel MMA device have been assessed and its performance has been evaluated under environmental constraints of a future space mission, in terms of temperature (from -40 °C to 80 °C), vacuum ($< 10^{-5}$ mbar) and vibrations in X-, Y- and Z-axes, showing zero failure rate for the MMA device after all tests. These experimental findings, together with simulations results, confirm the robustness of the MMA technology, especially against temperature changes, and encourage further activities for the development of a space-customized spatial light modulator technology.

Keywords: Spatial Light Modulator, Micromirror Array, MEMS, space deployment, Earth Observation, environmental tests

1. INTRODUCTION

Spatial Light Modulator (SLM) technologies have been well established in many application fields over the last decades [1]. Today, the main drivers for the application development in the mass markets of imaging and specific instrumentation comprise Digital Micromirror Device, Liquid Crystal Display and Liquid Crystal on Silicon devices.

In the past 30 years, the rapid development of micro-electromechanical systems (MEMS) has provided an important boost for the Micromirror Array (MMA) device, a reflective class of Spatial Light Modulator (SLM), giving rise to multiple MMA designs [1]. MMA devices developed at Fraunhofer IPMS have been successfully applied during the last decades in industrial photolithography tools, being fine-tuned to work in the ultraviolet spectral range. Nevertheless, further customizations of this MMA technology are possible in order to optimize the SLM characteristics for new emerging application fields, such as: laser beam steering [2], microscopy [3] and holography [4].

On the other hand, in the last years a significant growth of the possibilities of SLM devices has been observed in new research topics for space applications where SLM technologies provide an added value in crucial issues like mass, volume, power consumption and reliability. For example, MMAs bring benefits in the multi-object-spectroscopy in order to measure efficiently a large number of stars and galaxies [5]; in adaptive optics field, enabling wavefront error correction and improving the observation through inhomogeneous media [6]; and in planetary landing navigation where a MMA is the main component in optical correlators [7].

*sara.frances-gonzalez@ipms.fraunhofer.de; phone +49 351 8823-472; https://www.ipms.fraunhofer.de

This encouraging background inspired the present work, where in the framework of the EU H2020 SURPRISE project we have studied an optimized space-oriented MMA concept taking into account the specifications of a future Earth observation payload based on the compressive sensing paradigm and working in the mid-infrared spectral range [8], [9]. As a part of this study, we conducted several experimental tests on the currently available IPMS MMA technology in order to assess its performance while working beyond the standard conditions it was designed for. Previous studies strongly support this approach with the investigation of several SLM technologies for space instrumentation.

2. MICROMIRROR ARRAY DEVICES UNDER TEST

The 64k-MMA Customer Evaluation Kit (CEK) analysed in this study contains a Spatial Light Modulator (SLM), namely a MMA, and its electronic driver (Figure 1). Significant parts of its development have been carried out in the framework of a EU founded project, the MEMI project [10].

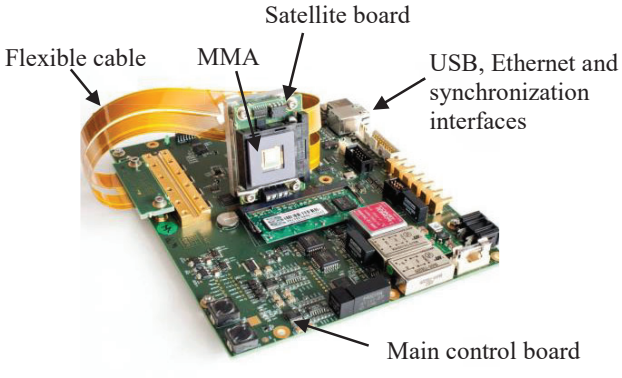

Figure 1 64k-MMA CEK with micromirror array device and electronic driver

The 64k-MMA CEK consists of an array of 256 x 256 tiltable micromirrors, each with a size of 16 µm, and the MMA electronic driver, which comprises a main control board and a satellite board, both connected by a flexible cable. The electronic driver allows the addressing of each micromirror independently, with the possibility to set a tilt angle from 0 ° to 3.5 °. The system is able to control the mirror tilt as a continuous function with variable addressing voltages as major input parameter (so-called analog deflection mode). By using this feature in combination with a proper optical system (Fourier optical system), a pattern generation with up to 256 grey levels in one laser pulse can be generated without time multiplexing or similar techniques [11]. The same technique can be used for the fine placement of pattern edges (white and black lines) within a subgrid in photolithography tools [12]. The MMA requirements for the application studied in the EU H2020 SURPRISE project are mainly dictated by its use as a core element of compressive sensing instrument, where only a binary deflection mode is required, that is, two mirror deflection states (ON and OFF) are sufficient for black-white image generation. The current available electronic driver can generate variable patterns with a frequency of up to 1 kHz.

Firstly, the functionality of the MMA was assessed in standard conditions. The advanced test set-up described in [11] was used in order to identify and characterize the MMA samples used in the experiments of Section 3, as well as to create some examples of binary and greyscale patterns as shown in Figure 2 and in Figure 3.

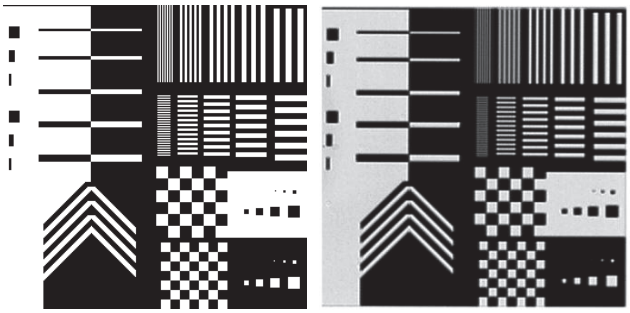

a) b)

Figure 2 Example of a binary pattern (black-white image): a) Original image and b) projected imaged using 64k-MMA

Figure 3 Examples of greyscale patterns created with a 64k-MMA

3. ANALYSIS AND TEST IN SPACE RELEVANT ENVIRONMENTAL CONDITIONS

The performance of Fraunhofer IPMS MMA technology under standard environmental conditions is well known. These conditions are similar in all different application fields for which this MMA technology was used up to now, specifically: atmospheric pressure and ambient temperatures in the range from 20 °C to 25 °C. In this section, we report the results of our investigation on the suitability of this MMA technology under space relevant environmental conditions, which was carried out for the first time. The outcome of these preliminary tests was not predictable due to the fact that the tested devices were not specifically developed for space applications. Nonetheless, the outcome of these tests are very valuable as inputs to develop an optimized MMA, customized for space applications, which will be extensively tested in the future.

Several SLM devices have been already tested for space applications [13]–[15]. Space environment can affect MEMS devices depending on their design, their materials or their packaging. The main failure modes are mechanical, like sticking or delamination, and electrical, for instance electrostatic discharge [16]. In this study, we investigated three aspects of space environmental conditions: temperature, vacuum and vibrations. Radiation is, of course, a further critical issue for space missions [17] and will be analysed for this MMA technology in detail in future activities. First radiation test experiments on other MMA technologies, however, have already been carried out in the past [18], [19].

3.1. Temperature Test

Two different approaches were followed to analyse the impact of the temperature in the MMA technology presented in this study: (1) theoretical investigations on the mirror deflection curves by means of Finite Element Method (FEM) based simulations, and (2) experimental tests by modifying the environmental temperature inside a climate chamber.

Theoretical investigations

The deposition of different layers in surface micromachining and successive processing steps cause at least a residual stress in the metal alloy of the actuator hinges. That layer is responsible for the mirror movement, and this stress impacts directly

on the deflection behaviour. This can be seen by a slight change of the natural frequency of torsion modes when changing intrinsic tensile stress. A temperature deviation causes the thermal expansion of the actuator hinges leading to a change of stress. Besides, there is a temperature dependency of the material properties like Young's or shear modulus, although that can be considered as negligible in the temperature range of interest.

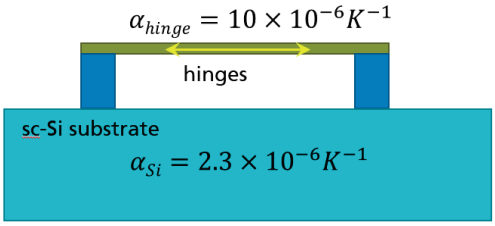

Figure 4 Side view of a hinge layer on Si-substrate with corresponding coefficients of thermal expansion, α_{Si} and α_{hinge}

In order to better evaluate these effects, an analysis by FEM simulations was carried out. The electrostatic force at a certain pixel electrode voltage and the resulting deflection state were calculated by using the so-called transducer FEM-elements provided by ANSYS®. A schematic of substrate and hinge materials and their corresponding coefficients of thermal expansion α can be seen in Figure 4. Being E_{hinge} the Young's modulus of the hinge, if the environment temperature changes, with $\Delta T = T - T_{ref}$, then the thermal stress σ_{th} in the hinge bars can be estimated as follows:

$$\sigma_{th} = (\alpha_{Si} - \alpha_{hinge})\, \Delta T\, E_{hinge}.$$

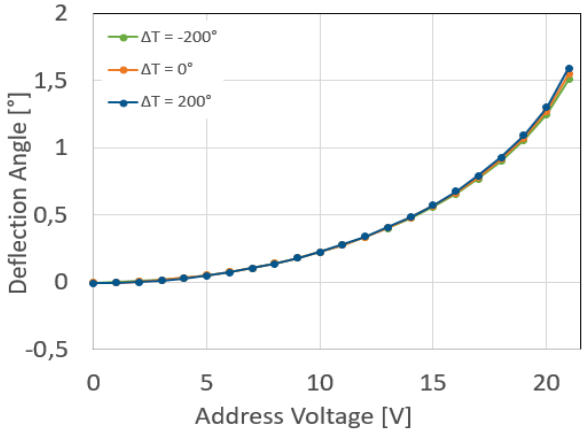

Figure 5 Electrostatic deflection curves for different temperature variation ΔT

Figure 5 depicts a characteristic curve for a single mirror of a 64k MMA and its temperature dependency. It indicates that the influence of the temperature on the electrostatic deflection is negligible over a wide range of voltages. The largest deviations occur at higher voltages: for instance, at 21 V, the tilt angle deviation is 0.03 ° or rather, 2 %, for ΔT values of -200 °C and 200 °C. This is because the torsion stiffness is affected by the stress along the torsion bar direction only to a minor extent, and consequently the electrostatic deflection state at temperatures different from T_{ref} differs only slightly from the reference one.

Temperature experimental tests

The DM250 C15 ESS climatic chamber from Angelantoni Test Technologies [20] was used to assess the performance of 64k-MMA in a temperature range from -40 °C to 80 °C at ambient pressure and ensuring a relative humidity < 10 %. The MMA device was covered with a non-hermetic glass window.

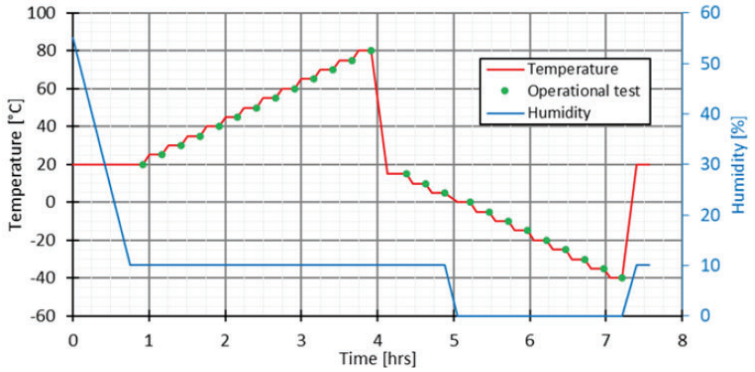

Figure 6 Test conditions and procedure for temperature check

A MMA sample was placed in the thermal chamber and the chamber environmental conditions were monitored by means of a Graphtec GL820 data logger with an acquisition frequency of 0.1 Hz. In order to properly measure the temperature of the chamber and of the device, two external platinum resistance thermometers PT100 were employed, one glued to the ceramic frame of the device and the other to the chamber. Operational verification tests were performed stepwise (Figure 6) after a constant temperature had been measured in both sensors for several minutes, in this way guaranteeing a thermal stabilisation of the device tested at each temperature step. During the experiment, we opted for a simple and compact experimental set-up which, although not allowing for an optimal MMA illumination, provided contrast enough to identify single mirror defects, yet fitting inside the climate chamber. The industrial camera Imaging Source DMK 33UJ003 [21] with a CMOS sensor of 3856x2764 pixels, combined with a Xenoplan 1.9/35-0901 lens (f/1.9), was employed to acquire monochromatic images that detect the single-pixel state changes.

To avoid damage of test equipment, two configurations were employed (Figure 7). For high temperatures, MMA and light source were located inside the thermal chamber, while the MMA electronic driver and CMOS camera were outside, with a direct line of sight through a lateral opening in the chamber. This arrangement prevented camera and electronics from operating outside their operational temperature range. On the contrary, for low temperatures the camera with thermal isolation was placed inside the thermal chamber, together with the SLM and a light source to prevent fogging effects in the chamber window.

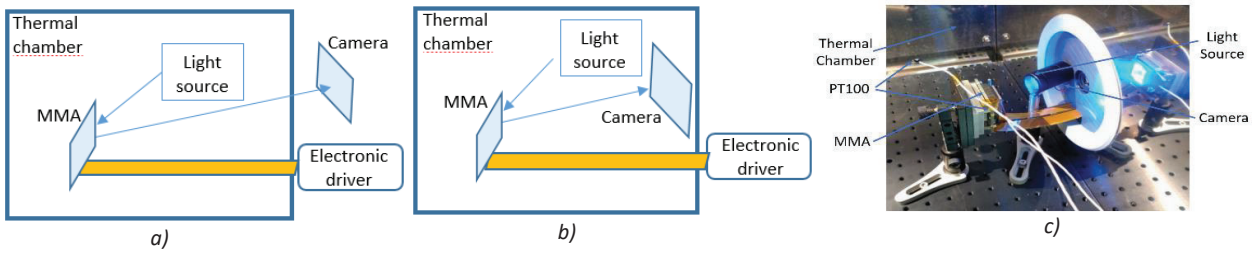

Figure 7 Temperature test configurations: a) high temperature set-up, b) low temperature set-up; and c) a view of laboratory set-up

During each temperature step, the MMA functionality was tested in the following sequence: firstly, two images were recorded with all micromirrors in ON and in OFF state (white and black picture) by using the CMOS camera. In order to identify non-working pixels, the image difference between white and black was calculated and, if the intensity value of a set of 3x3 pixels was lower than a given threshold, a non-working micromirror was detected. Thanks to the high pixel density of the employed camera, each micromirror can be mapped to at least 3x3 camera pixels. For the analysis, in order to avoid rounding errors, the monochromatic image was converted to floating point with values between 0 and 1; then the subtraction was made. Finally, they were converted to integer values (between 0 and 255) for plotting. The changes in intensity that can be observed by comparing these figures to those obtained in the experiments in following subsections, are due to modifications in the optical alignment and the distance between the elements. Specifically, we could not exactly

reproduce the same illumination conditions in all the experiments; this, however, does not affect to the detection of possible defect micromirrors. A calibration procedure was carried out upfront, changing intentionally the state of a single micromirror and it could be confirmed that the camera is able to detect single-pixel failures.

As an example, we report the functionality test at 80 °C in Figure 8. All tests carried out between -40 °C and 80 °C showed the same MMA performance, maintaining full functionality (zero failure rate) for the whole temperature range.

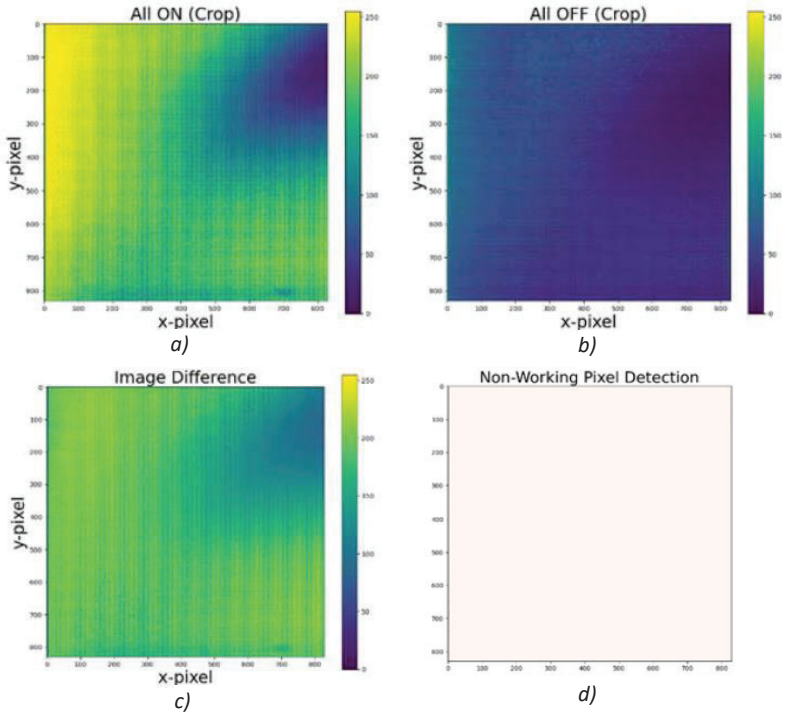

Figure 8 Functionality test at 80°C: a) recorded white image; b) recorded black image; c) calculated intensity difference between a) and b); d) matrix representation that would show defect mirrors, if there were any.

3.2. Vacuum Test

Vacuum experiment

We assessed the robustness of a MMA sample without any glass cover after being exposed to a low pressure environment, by means of a vacuum chamber with a custom pumping station featuring an Edwards XDS10 Dry Scroll primary pump and a Pfeiffer Balzers turbo pump (Figure 9). Before starting the experiment, the vacuum chamber and the MMA support were cleaned in a flow box (with clean room classification ISO 5) to remove dust and other contaminants. To ensure stable experiment conditions, the tests started after the pressure in the chamber remained constant ($< 10^{-5}$ mbar) at least for 2 hours at ambient temperature.

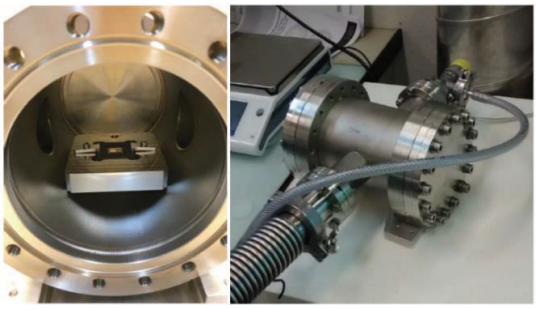

Figure 9 Test set-up with MMA in the vacuum chamber

Due to limited space for all relevant components inside the vacuum chamber, no MMA control and functionality test was applied due to limited space for all relevant components, but rather the operational MMA test was performed immediately after removing the device from the chamber. The functionality test is similar to the one used for the temperature experiment: two MMA patterns were applied, the relevant images recorded and the positions of non-working mirrors were identified, if any. Test results showed a zero failure rate of the MMA (Figure 10). This means all micromirrors were able to switch their state from ON to OFF before and after having been exposed to vacuum.

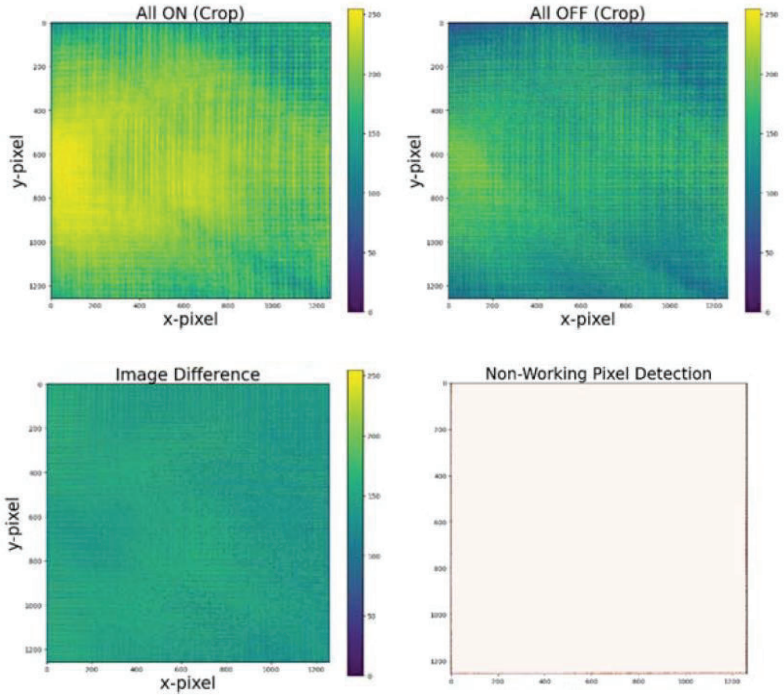

Figure 10 Functionality test after vacuum experiment

Challenging vacuum conditions entail an extensive and complex analysis, since changing damping conditions lead to different mirror oscillation times when the tilt angle is changed. At lower pressure the mirror damping decreases and the oscillation takes longer until the mirror remains in a stable position, therefore overall operation speed decreases. In addition, mirror overshoot with temporary high deflections during the mirror settling could occur, which might cause mirror failures in a worst case scenario. Hence, it seems sensible to keep standard atmospheric pressure, encapsulating the MMA device inside a hermetical package. Moreover, a hermetical solution would enhance the long-term reliability of the device, making possible a strengthened protection of the array surface against moisture and particles [16]. Operational tests in vacuum environment will be carried out in future activities by using a space-suitable hermetical MMA package.

Theoretical investigations: Hermetical package in vacuum

Pressure differences between inside (atmospheric pressure 1 atm) and outside (almost vacuum conditions) the MMA package are challenging for package components, especially for the window cover. For this reason, a FEM model for a given hermetical package was implemented to calculate the stress level and displacement on the window cover under vacuum environment. Figure 11 shows the FEM Model with a sapphire window in a Kovar frame on a ceramic chip carrier. No bonding layers to fix the window or other components were included in the model. Thanks to device symmetry, and in order to increase computational speed, only one quarter of the MMA package was considered. The assumed pressure difference of air between the encapsulated domain and the vacuum environment is $p = 1000\ hPa$.

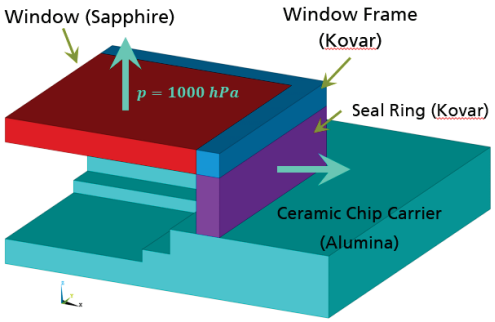

Figure 11 FEM Model for MMA hermetical package

The displacement of the window center u_z as well as the maximum total amount of the x-directed tensile stress component σ_{xx} is displayed in Figure 12 as function of the thickness of a sapphire cover window. Decreasing cover glass thickness increases glass displacement and tensile stress. Therefore, in order not to reach a stress level of approximately 270 MPa (Table 1) and to keep the risk of glass cracks very low, the glass thickness must be larger than 0.3 mm.

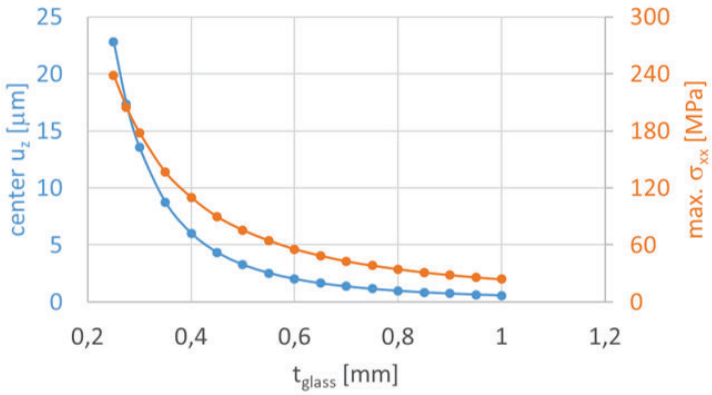

Figure 12 Maximum tensile stress (σ_{xx}) and center displacement (u_z) vs. window-cover thickness (t_{glass})

Table 1 Mechanical properties of Kovar (Fe/Ni/Co alloy) and Sapphire

Parameter	Unit	Kovar	Sapphire
Young's Modulus	GPa	207	345
Tensile Strength	MPa	518	270-410

3.3. Vibration Test

The vibration test determines the dynamic load that the MMA can withstand. To generate this load, in this test only random vibration between upper and lower frequency limits were exerted, as deemed the most critical for the device in a space application. Random vibration is more characteristic of modern-field environments produced by rocket engines [7]. To apply the required vibration levels, a LDS555 electro-dynamic shaker with an LDS PA1000L linear power amplified was employed. The MMA device was tested along the three axis directions: X, Y and Z, for 2 minutes each. The MMA was mounted in a specific bracket onto the shaker; this bracket can accommodate the device in different orientations as Figure 13 depicts. Additionally, a control accelerometer was mounted onto the shaker to control the vibration level applied onto the system.

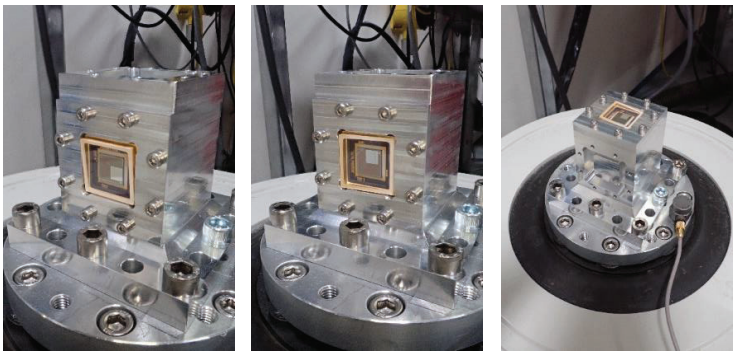

a) *b)* *c)*

Figure 13 Setup for vibration test along the three axis: a) X-axis, b) Y-axis and c) Z-axis

Various levels (Table 2) were tested in order to find a potential limit for acceptable vibrations and these levels correspond to those defined by the MIL-STD-883 specification method 2026 [22]. The root mean square acceleration (G_{rms}) is the square root of the area under the acceleration spectral density curve in the frequency domain. The G_{rms} value is typically used to express the overall energy of a particular random vibration event and is a statistical value used in mechanical engineering for structural design and analysis purposes [23].

Table 2 Test condition letters for Random vibration Test according to MIL-STD 883 Method 2026

Test Condition	Max. Amplitude [G^2/Hz]	Overall [G_{rms}]
1-A	0.02	5.2
1-C	0.06	9
1-E	0.2	16.4
1-G	0.4	23.1

In Figure 14 the target (green) and the actual (black) measured acceleration profiles in frequency domain are represented. It can be seen that the measured profile falls inside the tolerances (top and bottom yellow lines). MMA operational verification tests were performed before and after the test of each axis and they were successful (Figure 15), assuring the MMA functionality at least for the vibration condition 1-G. In order to check higher vibration levels in the future, additional testing on a more powerful shaker will be required.

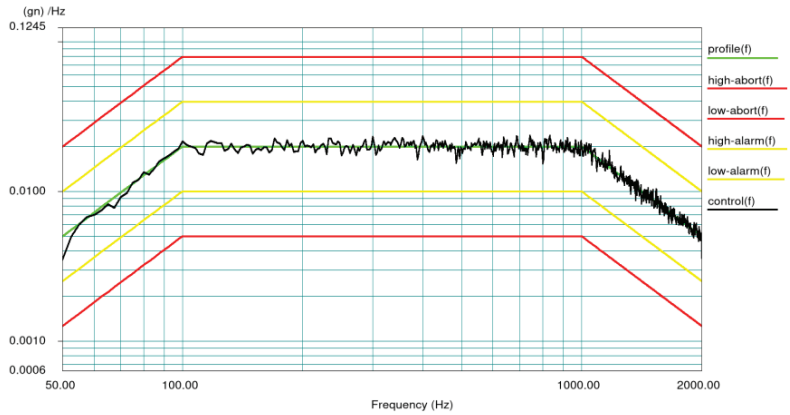

Figure 14 Example of a random spectrum for the test condition 1-G along X-axis

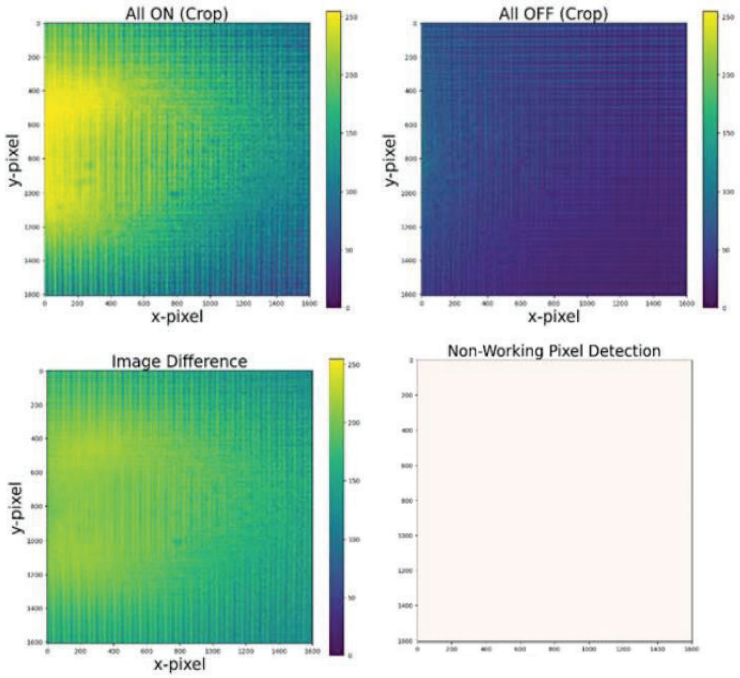

Figure 15 Functionality test after vibration experiment

4. CONCLUSIONS

In this paper, we reported on the first space relevant environmental tests, in terms of temperature, low pressure and vibrations, carried out on Fraunhofer IPMS MMA technology. Although the samples and electronic driver used in the experiments were not designed for space conditions, the results are very encouraging: all 256x256 mirrors of the tested device remained functional with zero failure rate after all the experiments. Furthermore, additional simulations and analysis have confirmed the robustness of this MMA technology against significant temperature changes and allowed to quantify features of a potential hermetical package, like the windows cover thickness. An opportunity for a space-customized spatial light modulator technology for the future seems closer than expected.

ACKNOWLEDGEMENT

This work is part of the SURPRISE project receiving funding from the European Union's Horizon 2020 research and innovation programme under Grant Agreement No 870390. Thanks to the SURPRISE project team for the fruitful discussions supporting the current work, to IPMS SLM development and fabrication teams for providing the test devices, and IPMS and CSEM lab teams for performing the experimental tests.

REFERENCES

[1] Song, Y., et al., "A review of micromirror arrays," Precision Engineering 51, 729–761 (2018).
[2] Gehner, A., et al., "Novel 512 × 320 Tip-Tilt Micro Mirror Array in a CMOS-Integrated, Scalable Process Technology," International Conference on Optical MEMS and Nanophotonics (OMN) (2018).
[3] Rückerl, F., et al., "Spatio-angular light control in microscopes using micro mirror arrays," Proc. SPIE 9305, Optical Techniques in Neurosurgery, Neurophotonics, and Optogenetics II (2015).
[4] Dürr, P., et al., "MEMS piston mirror arrays for computer generated holography," Proc. SPIE 12013, MOEMS and Miniaturized Systems XXI (2022).
[5] Lee, C. and Zhou, G. (eds.), [Optical MEMS, Nanophotonics, and their Applications], CRC Press (2018).
[6] Wu, J., et al., "Correction of Distorted Wavefront Using Dual Liquid Crystal Spatial Light Modulators," Photonics 9(6) (2022).
[7] Tchernykh, V., et al., [Optical Correlator based Optical Flow Processor for Real Time Visual Navigation], InTech (2007).
[8] "EU H2020 Project SURPRISE,", https://www.h2020surprise.eu/ (11th July 2022).
[9] Raimondi, V., et al., "Designing a Compressive Sensing Demonstrator of an Earth Observation Payload in the Visible and Medium Infrared: Instrumental Concept and Main Features,", 27.
[10] "EU-Project MEMI,", https://cordis.europa.eu/project/id/215597 (26 November 2021).
[11] Berndt, D., et al., "Multispectral characterization of diffractive micromirror arrays," Proc. SPIE 7718, Optical Micro- and Nanometrology III (2010).
[12] Dauderstädt, U., et al., "Advances in SLM development for microlithography," Proc. SPIE 7208, MOEMS and Miniaturized Systems VIII (2009).
[13] Travinsky, "Evaluation of digital micromirror devices for use in space-based multiobject spectrometer application," Journal of Astronomical Telescopes, Instruments, and Systems (2017).
[14] Zamkotsian, F., et al., "Space evaluation of 2048×1080 mirrors DMD chip for ESA's EUCLID Mission,", 773130.
[15] Silva-López, M., et al., "Validation of a spatial light modulator for space applications," Proc. SPIE 11180, International Conference on Space Optics (2018).
[16] Shea, H. R., "Reliability of MEMS for space applications," Proc. SPIE 6111, Reliability, Packaging, Testing, and Characterization of MEMS/MOEMS V (2006).
[17] Shea, H. R., "Effects of radiation on MEMS," Proc. SPIE 7928, Reliability, Packaging, Testing, and Characterization of MEMS/MOEMS and Nanodevices X (2011).
[18] Fourspring, K., et al., "Proton radiation testing of digital micromirror devices for space applications," Opt. Eng 52(9), 91807 (2013).
[19] Zamkotsian, F., et al., "Successful evaluation for space applications of the 2048×1080 DMD," Proc. SPIE 7932 (2011).
[20] Angelantoni Test Technologies, "Angelantoni Test Technologies,", https://www.acstestchambers.com/en/environmental-test-chambers/ (11th July 2022).
[21] The Imaging Source, "Industrial Cameras,", https://www.theimagingsource.com/products/industrial-cameras/ (15th July 2022).
[22] "MIL-STD-883,", http://scipp.ucsc.edu/groups/fermi/electronics/mil-std-883.pdf (11th July 2022).
[23] Wikipedia, "Random vibration,", https://en.wikipedia.org/wiki/Random_vibration (3rd June 2022).